A Quantitative Acoustic Microscope with Multiple Detection Modes

JONATHAN M. R. WEAVER, CHRISTOPHER M. W. DAFT, AND G. A. D. BRIGGS

***Abstract*—An acoustic microscope that permits operation with both toneburst and impulse excitation of the lens has been developed. Either mode may be switched-selected and combined with mechanical scanning in any direction. In impulse-excited mode, the specular and Rayleigh signals from the sample are resolved in time, and analysis is performed to obtain surface wave propagation parameters. The power of the simultaneous application of these techniques is illustrated by measurements on specimens of intact and fractured glass and duralumin-ium. Reflection and transmission coefficients for a crack are measured, and conclusions are drawn about $V(z)$ processing. These results are significant because the images of cracks produced by the conventional toneburst SAM tend to be complex. Previous work has, therefore, centered on crack detection, rather than characterization. Lastly, diffraction from the tips of cracks has been observed in the microscope.**

I. Introduction

In a typical high frequency reflection SAM the lens is excited by a narrow-band toneburst. The various signals from the sample interfere in the receiver filter. After demodulation and peak detection, the variations in phase between the components produce the characteristic oscillations in the $V(z)$ response [1]. An alternative approach is to excite the lens with a voltage spike to provide the shortest possible acoustic signal from the lens. This approach is common at low frequencies (up to 100 MHz) [2], and the resolution of such systems has been predicted [3]. In our experiment a lens with center frequency 250 MHz and useable output from 100 to 500 MHz was employed.

Two research groups have recently published work based around similar techniques. Gilmore *et al.* [4] at General Electric are using acoustic microscopy from 10 to 100 MHz for the support of automated manufacture. They demonstrated time-gated surface wave images which are useful for detecting cracks. Resolution and depth-of-field calculations were presented to evaluate the potential of the machine for volume inspection. Images of the interiors of solid objects, using the aspheric lenses of Pino *et al.* [5], provided information on the integrity of bonds between silicon wafers. This work reported here differs from that of Gilmore *et al.* in the frequency range used, and the focus of the work (crack characterization rather than crack detection, volume inspection and interior imaging).

Nikoonahad *et al.* [6] of University College, London, have addressed the problem of the large reflection at the surface/water interface, which complicates subsurface imaging in opaque objects. They applied the solution (pioneered in radar work) of supplying the lens with an expanded chirp pulse, which is then recompressed at the receiver. A 13-dB processing gain was achieved at a center frequency of 750 MHz, resulting in an improved capacity for broad-band interior imaging. Results were shown from semiconductors, and various types of debonded specimens.

Pulse compression was considered for the experiments in this paper. A problem with this approach is the signal-to-sidelobe ratio of suitable SAW filters. The value of this parameter for commercially available devices is typically 30 dB, which would cause severe problems in this application, due to the large dynamic range of the signals detected from our samples. Our substantially simpler system can also produce sufficient signal-to-noise ratio (SNR) for these measurements, due largely to the efficiency of the transducer. An equivalent data set could be obtained using the frequency domain techniques of Faridian and Somekh [7]. However, the rejection of spurious signals described in Section II would be harder to achieve.

II. The Instrumentation

Fig. 1. shows the arrangement of the impulse excited RF system. A step recovery diode (SRD) was used to produce a 5-V pulse with its width adjusted to be 1 ns, corresponding to a half cycle at the highest lens operating frequency. Since the signal to noise ratio is proportional to the integrated power of the transmit signal, using a faster pulse with the same peak voltage would degrade the noise performance. The acoustic lens was connected via a broadband single pole double throw p-i-n switch to a limiting amplifier. The amplifier's limiting level was adjusted so that the signals of interest were amplified without distortion, whilst the switching transients were clipped. All radio frequency (RF) components were selected to have a wider bandwidth than that of the signal, and to have a good impulse response. The output was fed

Manuscript received May 31, 1988; revised and accepted March 17, 1989. This work was supported by SERC, AERE Harwell, and GEC Hirst Research Centre.

J. M. R. Weaver is with IBM T.J. Watson Research Center, P.O. Box 218, Yorktown Heights, NY 10598.

C. M. W. Daft is with Department of Electrical and Computer Engineering, University of Illinois, 1406 W. Green Street, Urbana, IL 61801.

G. A. D. Briggs is with Department of Metallurgy and Science of Materials, University of Oxford, Parks Road, Oxford OX1 3PH, United Kingdom.

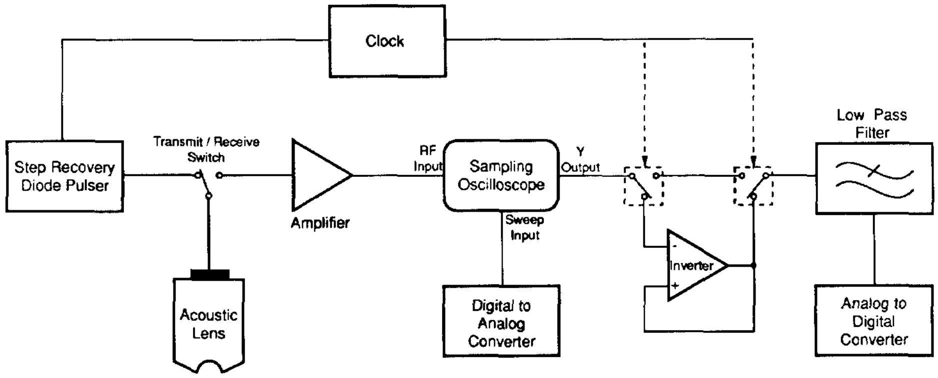

Fig. 1. Diagram of broad-band scanning acoustic microscope.

into a sampling oscilloscope, so the undemodulated RF signal from the lens could then be viewed. The time scan was driven by a DAC interfaced to a computer, and the output of the oscilloscope was collected by a 12-bit ADC. The system was configured with coaxial relays to permit instant selection of toneburst or impulse mode.

The main problem addressed by this RF system is the presence of many spurious signals. The p-i-n switch produces switching transients that not only feed directly into the amplifier, but also excite the lens transducer. These signals reverberate in the sapphire buffer rod and may be reflected from the specimen, mimicking the SRD-excited pulses. Since the system will detect signals considerably below the one-shot noise level, there are a large number of low-amplitude spurii that need to be separated from the desired signal.

Some form of background subtraction method was necessary (as in [2]) to remove from the final output all signals unconnected with the SRD pulse. The SPDT switch, gate and oscilloscope are triggered at 25 kHz, whilst the pulse generator is fired on every other clock pulse, i.e., at 12.5 kHz. The oscilloscope output is connected to a lock-in amplifier tuned to 12.5 kHz. This ensures that the ADC is oversampling, removes the background signal from the p-i-n switch, and also integrates over several pulses, reducing the detected noise level.

Reverberations due to the impedance mismatch at the transducer were minimized by connecting the lens to the SPDT switch with a very short piece of cable. Reflections due to other mismatches were separated from the desired signal by using 3-m cable runs from the other connections to the SPDT, and by resistive matching, where appropriate.

These procedures do not eliminate unwanted echoes derived from the transmit pulse. The reverberations from the previous transmit pulse were reduced by operating the microscope at a relatively low pulse-repetition frequency (PRF) (12.5 kHz). If higher accuracy is required, a background trace can be taken after moving the lens away from the specimen. This may then be subtracted in software.

A lens with 50 dB of insertion loss at its center frequency was used in the experiments. The one-shot signal to noise ratio in 500 MHz bandwidth, with the lens fo-

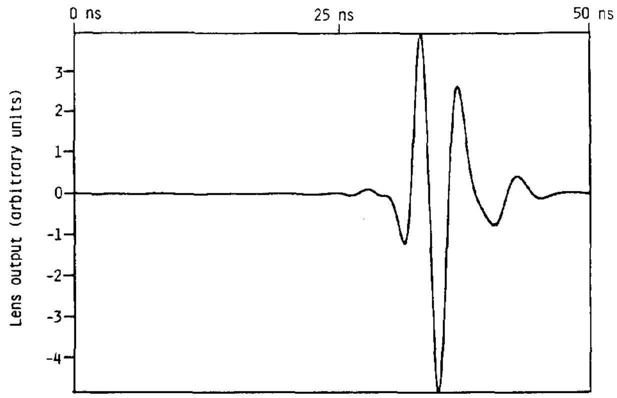

Fig. 2. Impulse response of system using glass slide reflector.

cused on a glass slide, is 43 dB. In the data given below, this figure is increased by signal averaging to provide accurate data when the microscope is operated at a substantial defocus, where the signals are smaller. Fig. 2 shows the impulse response of the system, measured at focus using a glass slide reflector. This system has been used to make measurements of the elastic properties of biological tissues [8], [9].

III. Separation of the Rayleigh Wave and Specularly Reflected Signals from a Glass Slide

When the acoustic microscope is used to image materials of high elastic modulus, leaky surface waves play an important role in the observed contrast. A convenient specimen is a glass microscope slide; this approximates to an isotropic half space. The Fourier optical formulation of the image contrast [10], [11] can be used to predict the microscope response for a given reflectance function. However, the ray model of Bertoni [1], gives a clearer intuitive understanding of the situation.

Fig. 3(a) shows the acoustic lens positioned at a negative defocus. The most significant rays that contribute to the SAM contrast are the specularly reflected ray [(a) in Fig. 4(a)] and the ray incident at the Rayleigh angle (b), which excites a leaky surface wave. Comparison of the

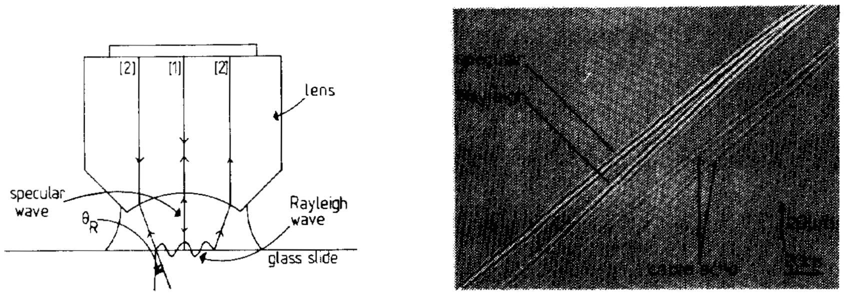

(a) (b)

Fig. 3. (a) Ray model of signals in hard sample. (b) $V(z, t)$ of glass slide.

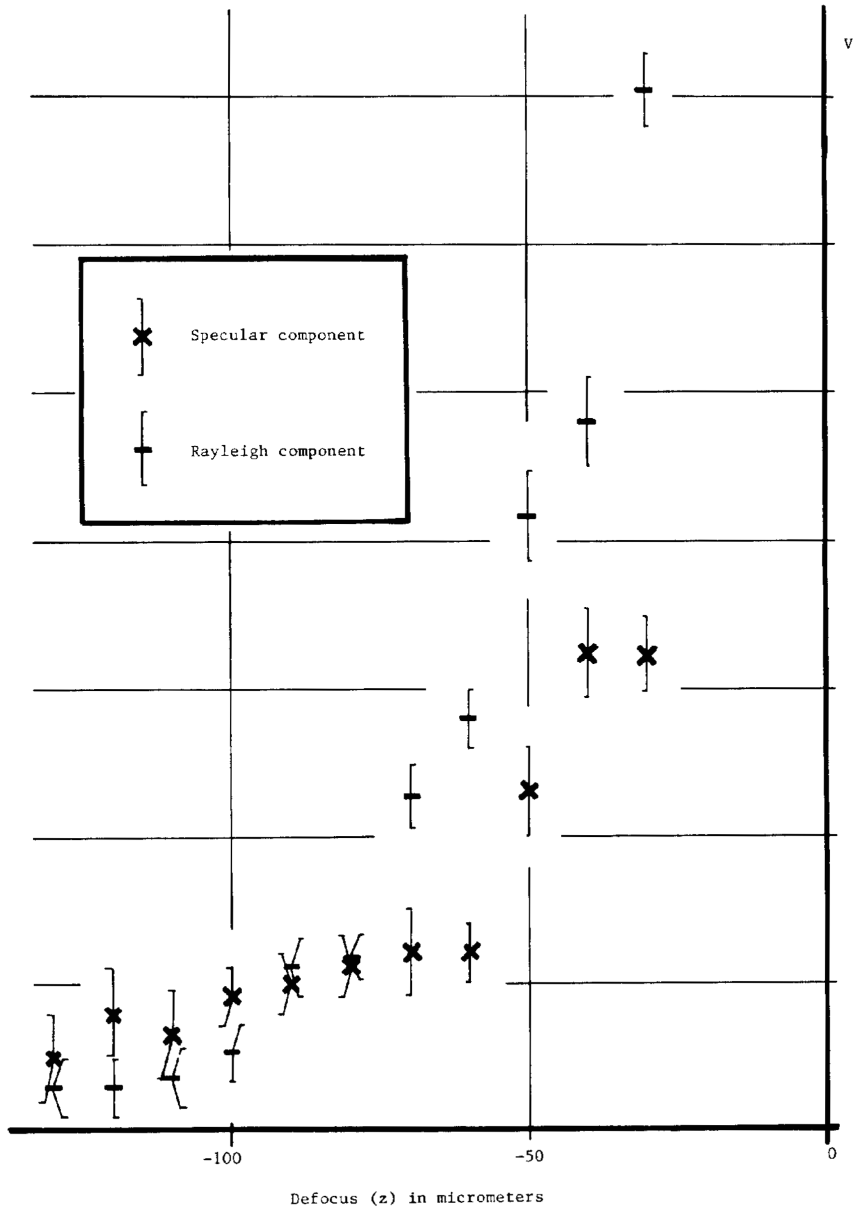

Fig. 4. The two components of $V(z)$ as determined from wide-band measurements.

path lengths reveals that the phase difference between the two rays is

$$\phi = 2\,kz(1 - \cos\theta_R) + \pi \tag{1}$$

where k is the wavenumber, z the defocus, and θ_R the Rayleigh angle for glass. This corresponds to a time difference of ϕ/ω, (where ω is the angular frequency) which is approximately proportional to defocus.

Fig. 3(b) shows pictorially the time resolved signal from the SAM as the defocus is varied from 0 μm (the top of the picture) to -150 μm (the bottom). The horizontal axis is time, with a field of view of 200 ns. Picture brightness is proportional to detected voltage, so the no-signal level is grey, and received signals appear as a succession of black and white stripes.

As the defocus increases, the specular and Rayleigh pulses separate; the Rayleigh signal is further to the right, due to its greater delay. The separation of the pulses in time is consistent with (1). A cable reverberation, caused by mismatches at the lens and the first amplifier, is also visible. It is separated in time from the signals of interest by the inclusion of 3 m of coaxial cable between the SPDT switch and the first amplifier.

The most significant conclusion to be drawn from these results is related to the relative amplitudes of the two components. In Fig. 4, the amplitudes are plotted as a function of defocus for polycrystalline dural, a material with similar acoustic properties to glass. At the small negative values of defocus at which the lens is typically operated, the Rayleigh signal in dural can be seen to be larger than the specular component. This has important consequences for the processing of toneburst $V(z)$ curves measured with spherical lenses. With cylindrical lenses, the effect of the Rayleigh wave signal is often treated as a perturbation [12]. Impulse excited measurements provide a useful check on the validity of this assumption.

IV. Characterization of Surface Breaking Cracks

The acoustic microscope has been found to be extremely sensitive to the presence of surface breaking cracks [2] due to the fact that such cracks are able to strongly scatter surface acoustic waves even when the width of the crack is small relative to an acoustic wavelength. While this has resulted in a relatively widespread use of the acoustic microscope in the detection of such cracks, the microscope has not generally been used to characterize them, due to the complex nature of the images produced [13].

There are expected to be four significant contributions to the measured signal (Fig. 5). First, there is the Rayleigh wave component transmitted through the crack (Fig. (a)). Next, there are two components reflected from the crack (Fig. (b) and (c)). There is also the specular component (Fig. (d)).

The temporal variation of specular and transmitted Rayleigh components with the defocus z is exactly as described above for an uncracked halfspace (1). This situation corresponds, in effect, to a crack with reflection and transmission coefficients for surface waves of 0 and 1, respectively. If the displacement of the crack from the lens axis is δx, the reflected components (Figs. (b) and (c)) will be detected at times $\pm 2\delta x / v_R$ relative to the transmitted Rayleigh signal. (v_R is the Rayleigh wave velocity.)

Fig. 6(a) shows the result of scanning the lens across a crack at a negative defocus. As before, time is the horizontal axis, displacement (δx) is the vertical axis and the received signal is mapped to brightness, with zero signal being mid-grey. The signal is shown schematically in Figure 6(b).

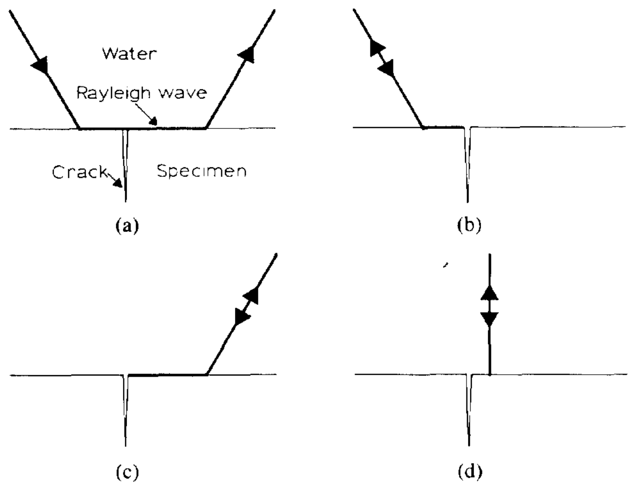

Fig. 5. Illustrating four most significant contributions to acoustic signal detected when wide-angle acoustic lens is scanned over surface-breaking crack. (a) Transmitted Rayleigh wave. (b) and (c) Reflected Rayleigh wave. (d) Specularly reflected component.

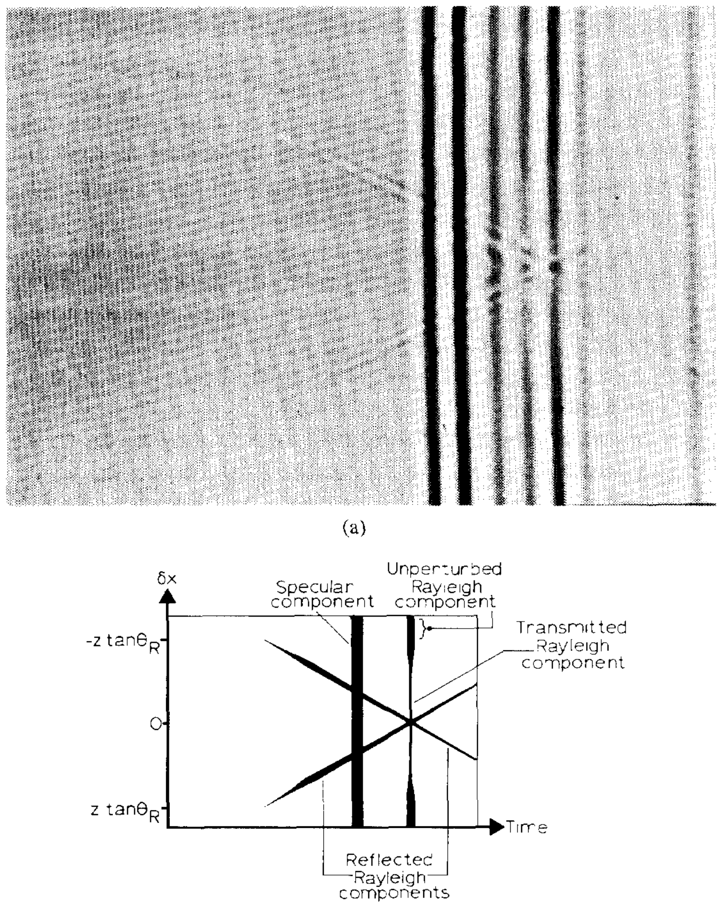

Fig. 6. (a) $V(x, t)$ plot over a crack in glass substrate. Center frequency, 250 MHz, $z = -100$ μm; water temperature = 52.5°C. Width of time scan = 100 ns; vertical scan size = 225 μm. (b) Schematic of (a), identifying four contributions to received signal.

To compute numerical values for the transmission and reflection coefficients for surface waves (respectively, T_s and R_s), we must first consider the paths followed by the reflected surface waves before detection (Fig. 7).

As surface waves are attenuated by reradiation, we need to ensure that the path lengths followed by both the transmitted and reflected waves are the same. Secondly, we must make certain that no wave is detected which has not either been reflected off or transmitted through the crack. Lastly, it is necessary that the detection of both transmitted and reflected Rayleigh waves be made with equal sensitivity. For all these reasons, the amplitude of transmitted and reflected Rayleigh wave amplitudes should be made by extrapolation to $\delta x = 0$.

In Fig. 8 the voltages are plotted as a function of δx, at times corresponding to the maximum and minimum excursions of the unperturbed transmitted Rayleigh signal. As the graph shows, for $|\delta x|$ greater than almost 50 μm the transmitted Rayleigh wave amplitude is approximately constant. In this case ($|\delta x| > -z \tan \theta_R$) the crack falls outside the Rayleigh wave excitation annulus, so that no perturbation of the transmitted Rayleigh wave pulse is found to occur. For $|\delta x| < -z \tan \theta_R$, an increasing proportion of the Rayleigh wave signal arises from waves transmitted through the crack, with the signal at $\delta x = 0$ resulting only from Rayleigh waves which have interacted with the crack.

Close to $\delta x = 0$, the delay between transmitted and reflected waves becomes small, and zero at $\delta x = 0$. The fast oscillations in signal near $\delta x = 0$ correspond to these reflected waves. By extrapolating the transmitted signal to $\delta x = 0$, and dividing its amplitude by the size of the signal far from the crack, we find that $T_S = 0.25 \pm 0.03$. If we equate the peak-to-peak excursion around $\delta x = 0$ (again normalized by the signal far from the crack) with $T_S + R_S$, we find that $R_S = 0.54 \pm 0.06$ for this crack. The sound which is neither reflected by, nor transmitted through, the crack is presumed to have undergone a mode conversion into bulk waves. Variations in both of these parameters have been observed from 0 to 1 with different cracks, suggesting that correlation with properties such as crack width and crack closure should be useful.

A particularly useful feature of pulse-excited measurements is that departures of the signal from the form predicted for simple cases is readily observed. In another measurement on the same specimen used in Fig. 6, a large asymmetry between the two reflected components was observed (Fig. 9). This corresponded to a crack which intersected with the surface at an angle other than 90°.

As a final example, the diffraction of surface waves about a crack tip have been observed using this system. This is an effect that has been studied extensively at lower frequencies (e.g., [14]). Fig. 10 shows a conventional toneburst SAM image of the tip of a crack, which exhibits the circular fringe pattern characteristic of crack tip diffraction effects. This fringe pattern arises from the inter-

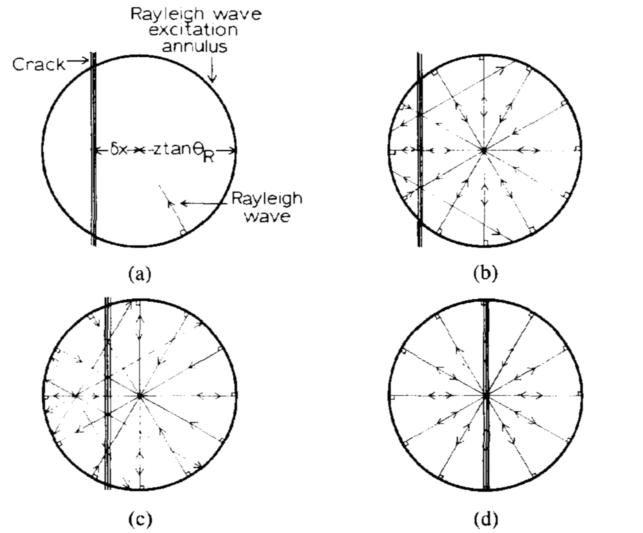

Fig. 7. Illustrating paths traced out, prior to detection, of surface waves in presence of a crack. Note that rays reflected from crack follow paths equivalent to transmitted and unperturbed rays only for $\delta x = 0$. (a) Definitions. (b) Reflected ray, $\delta x = 2(z \tan \theta_R)/3$. (c) $\delta x = (z \tan \theta_R)/3$. (d) $\delta x = 0$.

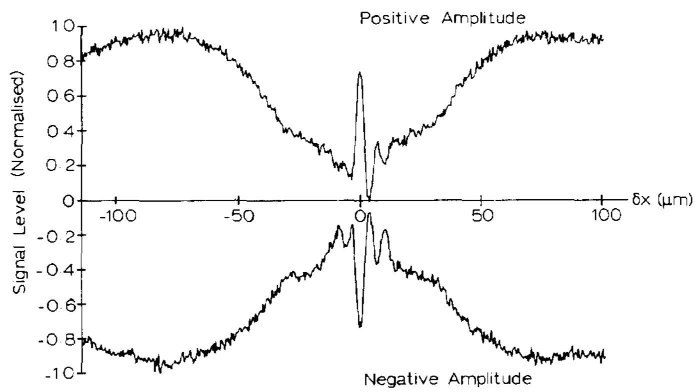

Fig. 8. Signal levels, measured at constant times, corresponding to maximum and minimum excursions of the transmitted Rayleigh pulse. Used in calculation of T_s and R_s (see text).

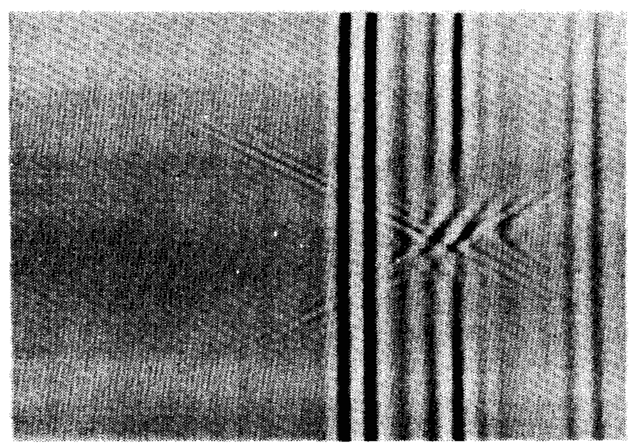

Fig. 9. $V(x, t)$ plot over crack in glass substrate showing high degree of asymmetry between reflected components.

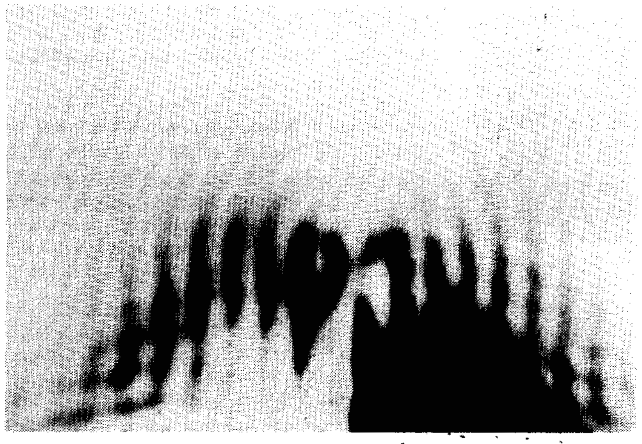

Fig. 10. Acoustic micrograph of indent in glass substrate. Field of view = 110 μm, $z = -100$ μm, frequency = 250 MHz, using water coupling at 52°C.

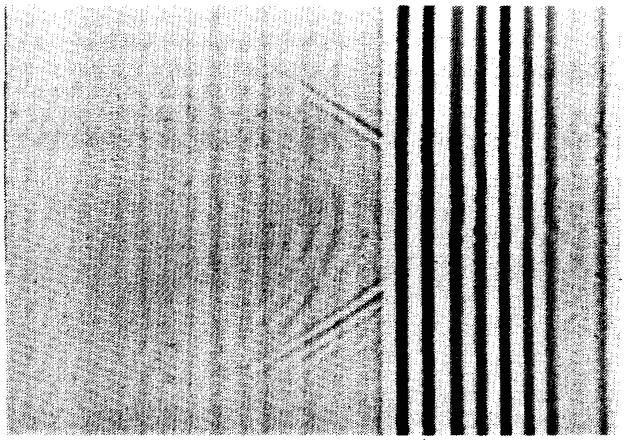

Fig. 11. $V(x, t)$ plot over specimen shown here. Width of time scan = 100 ns; vertical scan size = 220 μm. Note appearance of curved component, at time previous to reflected signals, corresponding to waves diffracted from tip of crack.

ference between Rayleigh waves scattered from the end of the crack and the other components described above. Due to their small amplitude, however, diffracted waves cannot be readily distinguished in the presence of the parallel fringes produced by the reflection of Rayleigh waves by the crack.

By making a measurement using impulse excitation, the diffracted wave may be readily distinguished by its characteristic curved form as the lens is scanned over the crack tip (Fig. 11). The tip of the crack scatters the Rayleigh waves from the lens, and behaves as a point source of sound. The diffracted wave is detected at the excitation annulus. Stationary phase arguments can be used to demonstrate that the received signal is dominated by the contribution from wavefronts parallel to the excitation annulus. When the crack is at the center of the annulus, the rate of change of the time position of the diffracted signal with δx is zero. This corresponds to the center of Fig. 9. In Fig. 11 we may also observe signals due to the transmitted and reflected Rayleigh components, and the specularly reflected component. Use of this technique may prove to be useful in the characterization of porous specimens, or those containing shallow cracks.

V. Conclusion

An acoustic microscope which permits rapid switching between toneburst and impulse excited modes has been described, and applied to the investigation of elastic discontinuities. Cracks are an obvious specimen for study in the SAM, due to their large influence on the detected signal. The use of impulse excitation greatly facilitates the interpretation of images and the quantitative characterization of these and other reflective features. However, the SNR is poorer because of the lower total energy in the signal exciting the lens, and the increased receiver bandwidth. This means that signal averaging is usually necessary, although a qualitative assessment of a region of the sample can be obtained in 20 s. By combining the diagnostic power of impulse excitation with the ability of a toneburst excited SAM to rapidly survey a specimen, and accurately measure velocity and attenuation, the characterization of complex specimens (e.g., dental enamel or soft tissue [15]) is greatly facilitated.

Acknowledgment

We are grateful to Drs. J. M. Rowe and M. G. Somekh for their valuable comments, and Dr. J. Kushibiki for providing the acoustic lens.

References

[1] H. L. Bertoni, "Ray optical evaluation of $V(z)$ in the reflection acoustic microscope," *IEEE Trans. Sonics Ultrason.*, vol. SU-31, pp. 105–116, 1984.

[2] K. Yamanaka, "Surface acoustic wave measurements using an impulsive converging beam," *J. Appl. Phys.*, vol. 54, pp. 4323–4329, 1983.

[3] M. Nikoonahad and E. A. Ash, "Resolution of scanning ultrasonic systems with arbitrary transducer excitation," *Revue Phys. Appl.*, vol. 20, pp. 383–389, 1985.

[4] R. S. Gilmore, K. C. Tam, J. D. Young, and D. R. Howard, "Acoustic microscopy from 10 to 100 MHz for industrial applications," *Phil. Trans. R. Soc. Lond. A.*, vol. 320, pp. 215–235, 1986.

[5] F. Pino, D. A. Sinclair, and E. A. Ash, "New technique for subsurface imaging using scanning acoustic microscopy," *Proc. Ultrason. Int.*, 1981, pp. 193–198.

[6] M. Nikoonahad, G. Yue, and E. A. Ash, "Pulse compression acoustic microscopy using SAW filters," *IEEE Trans. Sonics Ultrason.*, vol. SU-32, pp. 152–163, 1985.

[7] F. Faridian and M. G. Somekh, "Frequency modulation techniques in acoustic microscopy," *Proc. 1986 IEEE Ultrason. Symp.*, IEEE publication no. 86CH2375-4, pp. 769–773.

[8] C. M. W. Daft and G. A. D. Briggs, "Wideband acoustic microscopy of tissue," *IEEE Trans. Ultrason. Ferroelec. Freq. Contr.*, vol. 36, no. 2, pp. 258–263, 1989.

[9] C. M. W. Daft and G. A. D. Briggs, "The elastic microstructure of various tissues," *J. Acoust. Soc. Am.*, vol. 85, no. 1, pp. 416–422, 1989.

[10] K. K. Liang, G. S. Kino, and B. T. Khuri-Yakub, "Material characterization by the inversion of $V(z)$," *IEEE Trans. Sonics Ultrason.*, vol. SU-32, pp. 213–225, 1985.

[11] C. Chou and G. S. Kino, "The evaluation of $V(z)$ in a type II reflection microscope," *IEEE Trans. Ultrason., Ferroelec. Freq. Contr.*, vol. UFFC-34, pp. 341-345, 1987.

[12] J. Kushibiki and N. Chubachi, "Material characterization by line-focus-beam acoustic microscope," *IEEE Trans. Sonics Ultrason.*, vol. SU-32, pp. 189-212, 1985.

[13] G. A. D. Briggs and M. G. Somekh, "Acoustic microscopy of surface cracks: Theory and practice," in *Solid Mechanics Research for Quantitative Non-destructive Evaluation*, J. D. Achenbach and Y. Rajapakse, Eds. Dordrecht, The Netherlands: Martinus Nijhoff, 1987.

[14] M. G. Silk, "Changes in ultrasonic defect location and sizing," *NDT Int.*, vol. 20, pp. 9-14, 1987.

[15] G. A. D. Briggs, C. M. W. Daft, A. F. Fagan, T. A. Field, C. W. Lawrence, M. Montoto, S. D. Peck, A. D. Rodriguez, and C. B. Scruby, "Acoustic microscopy of old and new materials," in *Proc. 17th Int. Symp. Acoust. Imaging*, Sendai, Japan, 1988.

Jonathan M. R. Weaver was born in Stoke-On-Trent, England, in 1961. He received a B.A. degree in physics in 1982 from Oxford University, England, and a Ph.D. from the Department of Metallurgy, Oxford University, in 1986. His thesis work was concerned with the development of acoustic microscopy techniques for the study of plastic deformation in metals.

During 1986 and 1987 he was involved with the construction of a scanning tunnelling microscope, also in the Metallurgy Department.

Dr. Weaver is currently working at the IBM T.J. Watson Research Center on nanoprobe techniques.

Christopher M. W. Daft was born in Dundee, Scotland, in 1963, and received the B.A. and D. Phil. degrees from Oxford University in 1984 and 1987, respectively.

In 1987 he joined the Bioacoustics Research Laboratory of the Department of Electrical and Computer Engineering at the University of Illinois, Champaign-Urbana, as a Visiting Assistant Professor. His research interests include acoustic microscopy, ultrasonic dosimetry, tomography and tissue characterization, and neural networks.

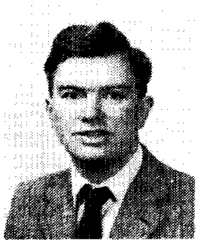

G. A. D. Briggs received his B.A. degree in physics at Oxford University, Oxford, England, in 1971 and his Ph.D. degree in physics at Cambridge University, Cambridge, England in 1976.

In 1980 he returned to Oxford to develop applications of acoustic microscopy to materials science. In 1982 he was appointed Royal Society Research Fellow in the Physical Sciences, and in 1984 he became a Lecturer in Metallurgy at Oxford University and a Fellow of Wolfson College at Oxford. He is on the Council of the Royal Microscopical Society and Chairman of the Materials Section, and he has written the Royal Microscopical Society Handbook on Acoustic Microscopy.